A General Strategy for the Preparation of ~~Ultrastable~~ Stable Luminous Nanocomposite Inks Using Chemically Addressable $CsPbX_3$ Peroskite Nanocrystals

Aizhao Pan,[†] Jianli Wang,[†] Matthew J. Jurow,[‡,#] Mengjun Jia,[†] Ya Liu,[$] Youshen Wu,[†]

Yanfeng Zhang,[†] Ling He,[*,†] and Yi Liu[*,‡,#]

†Department of Chemistry, School of Science, Xi'an Jiaotong University, Xianning West Road, 28, Xi'an, 710049, China.

‡The Molecular Foundry, Lawrence Berkeley National Laboratory, Berkeley, California 94720, United States.

#Materials Sciences Division, Lawrence Berkeley National Laboratory, Berkeley, California 94720, United States.

$ International Research Center for Renewable Energy, State Key Laboratory of Multiphase Flow in Power Engineering, Xi'an Jiaotong University, Shaanxi 710049, China

~~*KEYWORDS perovskite nanocrystals, environmental stability, light-emitting diodes, solution processable, nanoparticle ink*~~

ABSTRACT: The potential optoelectronic applications of perovskite nanocrystals (NCs) are primarily limited by major material instability arising from the ionic nature of the NC lattice. Herein, we introduce a facile and effective strategy to prepare extremely stable $CsPbX_3$ NC-polymer composites. NC surfaces are passivated with reactive methacrylic acid (MA) ligands, resulting in the formation of homogenous nanocubes (abbreviated as MA-NCs) with a size of 14-17 nm and a photoluminescence quantum yield (PLQY) above 80%. The free double bonds on the surface then serve as chemically addressable synthetic handles, enabling UV-induced radical polymerization. Critically, a bromide-rich environment is developed to prevent NC sintering. The composites obtained from copolymerizing MA-NCs with hydrophobic methyl methacrylate (MMA) and methacrylisobutyl polyhedral oligomeric silsesquioxane (MA-POSS) monomers exhibit enhanced properties compared to previously reported encapsulated NCs, including higher QYs, remarkable chemical stability towards water, and much enhanced thermal stability. The good solubility of the composite in organic solvent further enables its use as a solution processable luminescent ink, used here for fabrication of white light-emitting diodes (WLED) with high luminous efficiency and excellent color rendering index. The resulting fluorescent and stable NC ink opens the door to potential scalable and robust optoelectronic applications.

INTRODUCTION

Lead halide AMX_3 (A = cation, M = Pb, X = Cl, Br, I) type perovskite nanocrystals (NCs) exhibit exceptional optoelectronic characteristics and photovoltaic performance that may allow them to rival or even exceed traditional semiconductor nanocrystals for optoelectronic applications, including light-emitting diodes (LED), lasers, solar cells, photodetectors and display backlights.[1-6] Great efforts have been devoted to improving and stabilizing the high photoluminescence quantum yield (PLQY), narrow spectral widths, colloidal dispersability while improving our understanding of the fundamental optoelectronic processes in which these properties are grounded.[5-8]

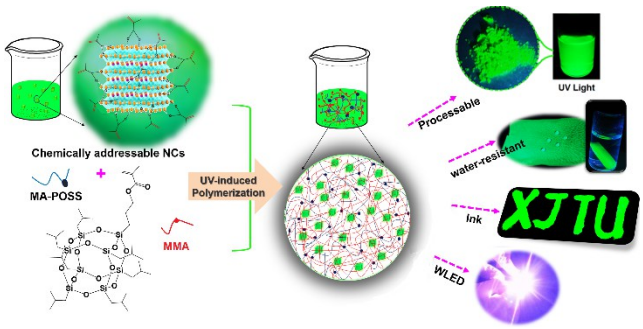
Compared to organic cation based analogues, all-inorganic $CsPbX_3$ (X=Cl, Br, I) perovskite NCs have superior PLQY and better stability.[5, 7, 9] $CsPbX_3$ NCs can be synthesized on a wide range of length scales by controlling the synthetic conditions and composition of surfactant ligands to yield various morphologies such as cubes, platelets, wires and spheres.[5, 10-12] Applications of

colloidal $CsPbX_3$ NCs are limited by the materials' instability towards moisture, heat, light and chemicals.[13-16] In most cases, exposure produces energy shifting, luminescent peak broadening, severe PL quenching and unacceptably short device lifetimes. The instability originates from the low formation energy of $CsPbX_3$ NCs, also responsible for the simple synthetic route to colloidal solutions.[14, 17, 18] Additionally, the ionic nature of perovskite NCs makes their ligands very labile and sensitive to polar solvents and environmental humidity.[19-21] Color purity and stability are further deteriorated by facile halide anion-exchange reactions of which mixed-anion $CsPb(X/Y)_3$ (X/Y =Cl, Br, and/or I) NCs are created.[7, 8, 18]

Recent efforts to improve perovskite stability are well reviewed, but are far from complete.[16, 20-23] Regulating surface ligands is a common technique to improve stability, including the inclusion of long-chain, branched or sterically hindered surfactant as capping ligands to create hydrophobic passivation layers around the NCs and impart tolerance to humidity.[16, 23-27] Specifically, branched (3-aminopropyl) triethoxysilane (APTES),[28] sterically demanding polyhedral oligomeric silsesquioxane (POSS),[16] ammonium bromide frameworks (NH_4Br),[29] alkyl phosphate[23] and phospho-silicate glass[30] were employed as passivation layers to improve stability of colloidal perovskite NCs, yielding materials stable in water for several days.

Incorporating NCs into a hydrophobic polymer matrix is another effective strategy to protect the NCs.[22, 31-34] Incorporating $CsPbX_3$ NCs into hydrophobic matrices of polystyrene (PS) can dramatically enhance the NC's stability towards light and water.[31] Highly luminescent perovskite/PS composite beads with good water stability and uniform morphology can be achieved by a simple swelling-shrinking strategy.[22] Additionally, various polymers such as PVP/silicone resin[34] and block copolymer of PS-b-PVP micelles[35] also effectively improve perovskite NC stability by providing a physical barrier for water permeation.

Blending NCs with polymers often results in unacceptably phase separated materials with grain size variations and agglomeration of NCs, broad PL peaks, low PLQY and unsatisfactory stability. To produce homogenous and stable NC/polymer composites, we focus on POSS-based polymers as an encapsulation layer. POSS-based polymers have been widely adapted in hybrid materials to induce hydrophobicity, and good mechanical and thermal properties,[36-38] owing to the three-dimensional cube-like silsesquioxane cage structures for the inorganic-particle effect and steric effect, and its low surface energy for hydrophobic passivation layer.[36, 37, 39-42]



Scheme 1. The design of PMPOPNC by *co*-polymerization with chemically addressable NCs

Herein, a new approach is developed to interface $CsPbX_3$ NCs with polymers by co-polymerizing methacrylic acid capped NC (MA-NC) with POSS-appended methacrylate monomer (MA-POSS) and/or methyl methacrylate (MMA) (Scheme 1). We have demonstrated that the use of the bifunctional MA ligands can effectively passivate the perovskite NCs by coordination surface atoms with the ligand's terminal carboxylate group. Critically, to prevent reconstruction of NCs into larger crystalline objects, a process that frequently results in a loss of luminance and stability, we developed a synthetic approach employing a bromide-rich reaction medium that effectively suppresses aggregation, allowing for the photo-polymerization of MA-NCs with *co*-monomers without degrading the nanocrystals. The resulting composite PMMA-*co*-P(MA-POSS)-*co*-P(MA-NC) (named PMPOPNC) is composed of uniformly distributed monodisperse NCs within the polymer matrix. The composite exhibits a high PLQY and extraordinary stability towards water and other protic solvents. Furthermore, the PMPOPNC composite can be dispersed in organic solvents to form easily processable inks. The great potential of PMPOPNC composite as a solution castable luminescent ink is demonstrated by its use as a green fluorophore in a white light emitting diode (WLED) device. This work presents an effective strategy to equip perovskite NCs with chemically addressable surface ligands for further chemical transformations.

RESULTS AND DISCUSSION

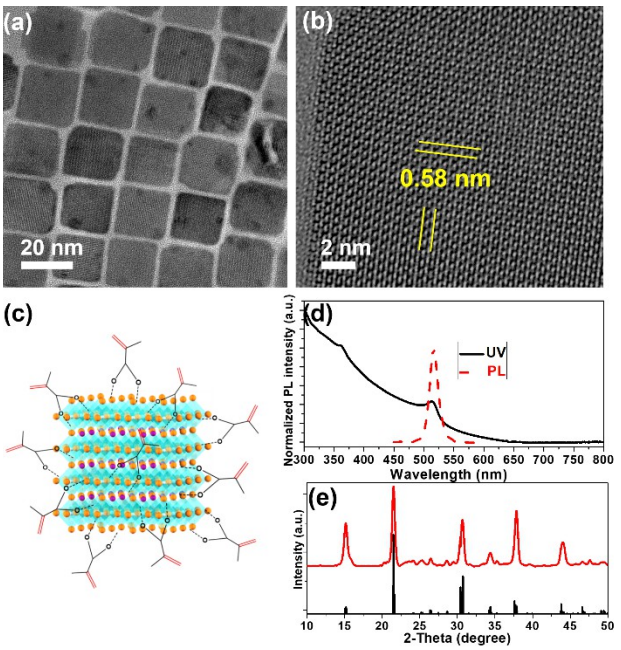


Figure 1. (a) Low- and (b) high-resolution transmission electron microscope (TEM) images of the MA-NCs modified with polymerizable surface ligands. (c) Schematic illustration of the MA-NCs decorated with polymerizable surface ligands. (d) Optical absorption and PL emission spectra of MA-NCs. (e) XRD pattern (Cu K) of MA-NCs (red) with the standard XRD pattern of orthorhombic of $CsPbBr_3$ (black).

In the well-established protocol for the synthesis of $CsPbBr_3$ NCs, both oleic acid and olelylamine are used as passivating ligands to solubilize the precursors and stabilize the colloidal NCs.[5, 7, 8] In our attempted synthesis of functionalized NCs, methylmethacrylic acid (MA) was used to replace the oleic acid and paired with either hexylamine (HAm) or olelylamine (OAm). The successful MA-capping of the nanocrystals was verified by the 1H-NMR and infrared (IR) transmittance spectra of the nanocrystal samples (Figure S1). The two resonances at 5.20 and 6.20 ppm present after extensive solvent washing with hexane and acetone, are assigned to the characteristic

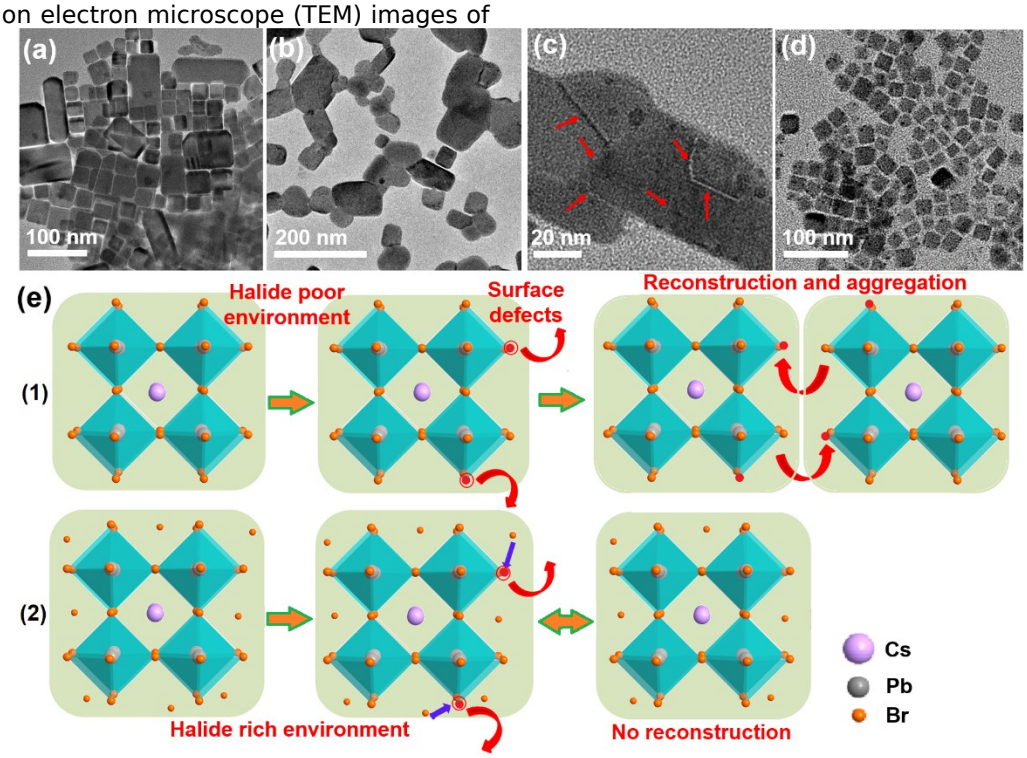


Figure 2. TEM images of MA-NCs after UV-light irradiation for (a) 30 min and (b) 60 min; (c) HR-TEM images of MA-NCs after UV-light irradiation for 60 min. Arrows indicate step edges from crystal reconstruction; (d) TEM images of MA-NCs after UV-light irradiation for 60 min in a Br-rich medium; (e) Schematic illustration of the mechanism of the UV light-induced changes of $CsPbBr_3$ NCs under Br-poor or -rich circumstances.

alkene protons from MA. As reported previously, the surface-bound ammonium ions were detached from the surface during the acetone wash, indicated by the absence of resonances from the amine ligands.[10] IR spectra of cleaned nanocrystals made with MA/OAm ligands also feature peaks corresponding to the loss of the ammonium N-H species and concurrent retention of the carboxylate ligands (Figure S1b).[10, 43] These results are consistent with previous findings that the stronger carboxylate surface ligands remain immobilized.

Figure 1a shows the transmission electron microscopy (TEM) images of the $CsPbBr_3$ nanocubes with MA/HAm ligands. Cubes have well-defined edges with lengths of 14-17 nm (Figure S2), larger than the $CsPbBr_3$ nanocubes obtained from the common OA/OAm mixtures (8 nm), a trend similar to other reported examples using shorter chain ligands.[5, 6, 44, 45]

The crystallinity is clearly verified by high-resolution TEM (HR-TEM) with a d spacing of 5.8 Å, corresponding to the (001) crystal lattice planes (Figure 1b).[10, 11] The bulk crystallinity of the MA-NCs were characterized by powder X-ray diffraction (PXRD) (Figure 1e), showing strong scattering signals that were consistent with the corresponding standard orthorhombic crystal phases of $CsPbBr_3$ NCs.[5, 7, 10] The UV-Vis absorption and photoluminescence (PL) properties of the MA-NCs (MA/HAm) show an absorption onset and PL emission peak at 512 nm and 515 nm, respectively, and a PLQY value near 85% (Figure 1d).

Irradiation is known to induce aggregation and reconstruction of perovskite NCs with neighboring particles, confirmed by our TEM studies.[14, 46, 47] Figure 2 shows the structural and morphological changes of MA-$CsPbBr_3$ NCs induced by UV light excitation over time. Compared with the initial well-defined quasi-cubic morphologies of MA-NCs (14-17 nm), some long rod-like aggregates are observed after 30 min UV light irradiation. The degree of aggregation increases with further UV excitation, although the crystal phase and lattice spacings remain unchanged (Figure S3a). It has been hypothesized that because the $CsPbBr_3$ NCs are ionic and the surface ligand-NC interactions are highly dynamic,[43] the UV irradiation causes the dissociation of the surface halides and ligands, creating an artificial bromide-poor environment (Figure 2e). The crystal facets with open sites are prone to recombine with nearby nanocrystals due to high ion mobility, thus reconstruction occurs to give larger crystals.[46, 48] The photon driven transformation is also supported by the step edges observed in large nanocrystals in TEM (Figure 2c).[48]

To overcome the photo-induced crystal reconstruction, we hypothesized that a Br-rich medium would restrict the fusion of neighboring nanocrystals by filling the surface bromide defects (Figure 2e). It was shown before that halomethanes can be photo reduced to generate halides in the presence of perovskite nanocrystals.[18, 49] Carbon tetrabromide (CBr_4, 10 mg) was thus added into the solution (2 ml, 0.5 mg/ml toluene with MA-NCs) as the photogenerated Br source to maintain a Br-rich environment. TEM image of the Br-rich MA-NCs that was irradiated under UV light for 60 min revealed that these NCs maintained their morphology and monodispersity (Figure 2d). The corresponding PL results indicate significantly decreased luminescence of MA-NCs after UV light irradiation for 30 min in the absence of CBr_4, while the MA-NCs irradiated under UV light for 60 min in Br-

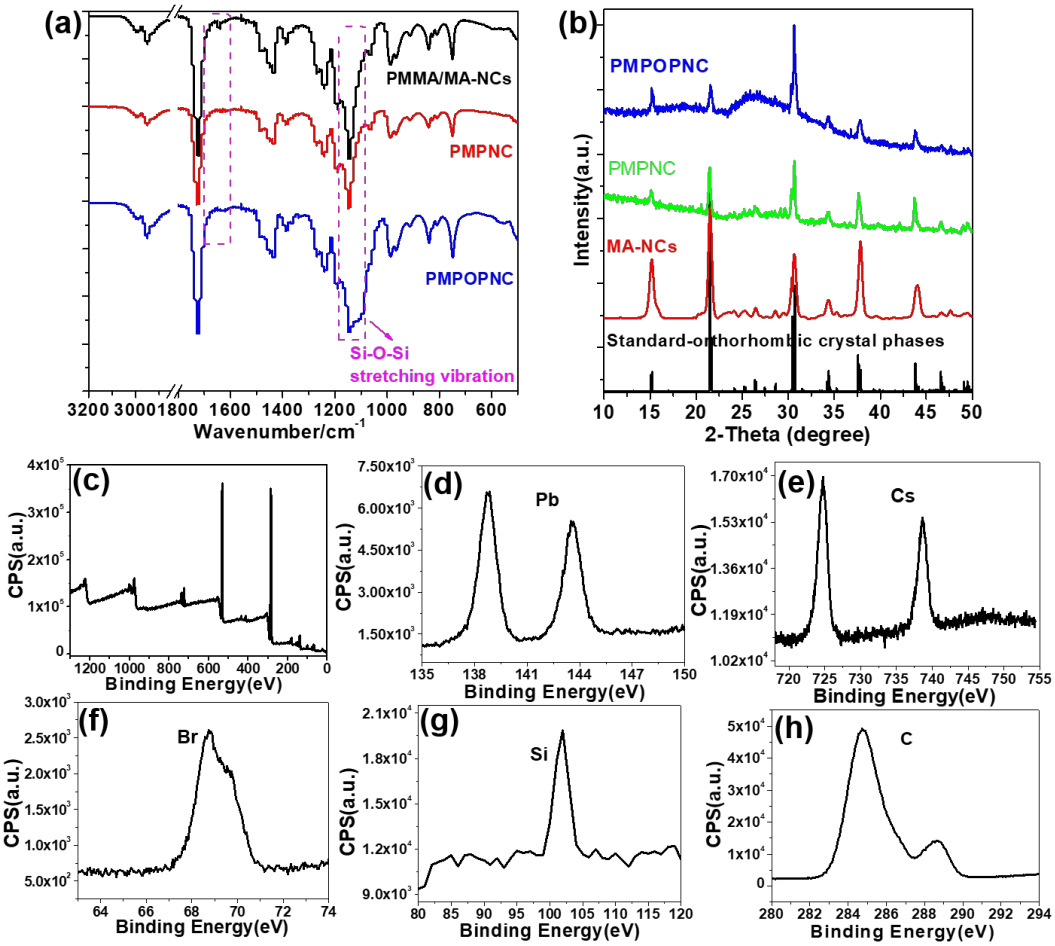


Figure 3. (a) IR spectra of the MA-NCs/PMMA mixture, PMMA-*co*-P(MA-NCs) (PMPNC) and PMPOPNC. (b) XRD pattern of MA-NCs, PMPNC and PMPOPNC, and also the standard orthorhombic crystal structure of $CsPbBr_3$. High-resolution X-ray photoelectron spectra (XPS) analysis of PMPOPNC powder showing (c) a survey scan and (d-h) zoom-in scans highlighting Pb, Cs, Br, Si and C elements.

rich medium remains highly luminescent, as observed from the optical pictures in Figure S3b. Clearly, maintaining a Br-rich environment is advantageous for passivating the surface defects and ensuring a high QY, thus sets the stage for the synthesis of composites via further photo-initiation polymerizations. The generality of this halide-rich stabilization effect for mixed halide systems was demonstrated in MA-$CsPb(Cl/Br)_3$ nanocrystals using a 1:1 mixture of CBr_4/CCl_4 (Figure S4). The morphology, monodispersity and PL peak position remain unchanged after an hour of UV irradiation.

The perovskite-based copolymers were thus synthesized by using MMA or a mixture of MMA and MA-POSS as monomers and AIBN as initiator at room temperature by photo-initiation, named as PMMA-*co*-P(MA-NC) (PMPNC) and PMMA-*co*-P(MA-POSS)-*co*-P(MA-NC) (PMPOPNC), respectively. Chemical evidence of co-polymerization with monomers is provided by IR and high-resolution X-ray photoelectron spectra (XPS) analysis. In a control sample made from physically blended MA-NC and PMMA, the IR spectrum (Figure 3a) shows that the C=C stretching signals appear at 1611 cm^{-1}, along with the intense absorptions at 2925, 2853, and 1300-1500 cm^{-1}, which are attributed to the C-H stretching and bending vibration from PMMA and MA ligands. In contrast, the C=C stretching signals in PMPNC and PMPOPNC disappear, and a broad Si-O-Si vibrational peak is observed at 1300-1500 cm^{-1}. The bulk crystallinity of the final composites by PXRD demonstrates that the diffraction patterns of PMPNC and PMPOPNC remain unchanged, corresponding to the orthorhombic crystal structure of perovskite NCs (Figure 3b).[5, 10, 11] XPS analysis of PMPOPNC (Figure 3c-h) further confirms that the elemental composition of the PMPOPNC powder contains all the elements expected from the $CsPbBr_3$ NCs, surface ligands, PMMA and POSS. The elemental ratio for Cs:Pb:Br measured by XPS amounts to 1:1:3.1 (Figure S5), which matches well with the expected ratio. The size distribution analysis of the original NCs and the solution of PMPOPNC by dynamic light scattering (Figure S6) demonstrate that PMPOPNC has a larger average size of 68 nm and a wider size distribution than the free MA-NCs. All these results are consistent with the formation of NC-polymer composites.

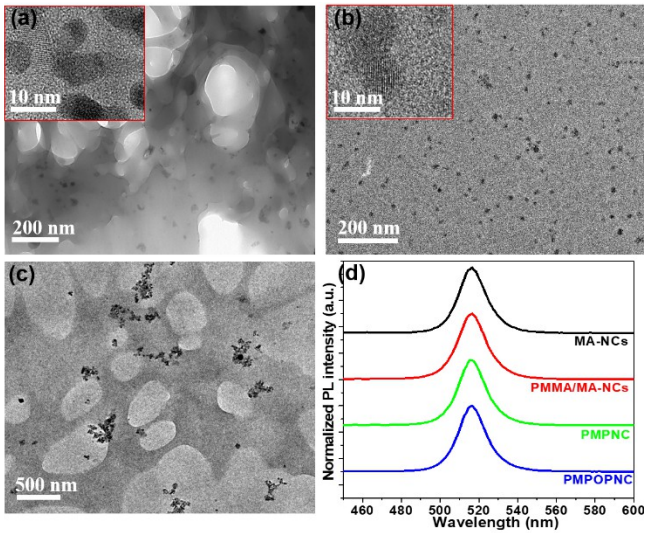


Figure 4. TEM of as-prepared composites of PMPOPNC cast from (a) hexane suspension and (b) toluene solution, and (c) control sample from blending of MA-NCs/PMMA casted from hexane. Insets in (a) and (b) are the corresponding HR-TEM images. (d) PL emission spectra of MA-NCs, MA-NCs/PMMA, PMPNC and PMPOPNC films.

TEM of PMPOPNC thin films cast from dispersions in hexane (Figure 4a) showed that the composite was composed of well-dispersed crystalline nanoparticles embedded within the amorphous PMMA-*co*-P(MA-POSS) (PMPO) matrix, distinct from the obvious phase separation and irregular aggregates observed in MA-NCs/PMMA blend (Figure 4c) and PMPNC made under Br-poor conditions (Figure S7a and S7b). The much better dispersion of NCs within the polymer matrix in PMPOPNC is also consistent with the fact that the Br-rich medium helps maintain the passivation of the NC surface. The films cast from toluene solutions (Figure 4b) showed dispersed black nanoparticles with sizes of ~12 nm within the matrix,[33, 45] with crystalline lattices identified by HR-TEM (insert in Figure 4b).[10, 11] The surface and cross-sectional morphologies of the thin films of different composites were also analyzed by scanning electron microscopy (SEM) and scanning transmission electron microscopy (STEM, see Figure S8). The surfaces of PMPNC and PMPOPNC films show a uniform morphology with several visible NCs crystals embedded in the polymer matrix (Figure S8), contrasted with the smooth morphology of PMMA and the rough morphology of MA-NCs/PMMA blend films with aggregated NCs. The cross-sectional SEM of PMPOPNC films indicate a thickness of ~7 μm and a uniform morphology decorated with visible NCs (Figure S9). These morphology results confirm that the

nanocrystals are embedded in the polymeric matrix with preserved sizes and shapes.

The fluorescence spectra of both films of PMPNC and PMPOPNC exhibited an emission peak at 516 nm, nearly matching that of the free MA-NCs and the MA-NC/PMMA composites (Figure 4d). Additionally, the PLQY of PMPNC (68%) and PMPOPNC (72%) films exhibited little change compared with the free MA-NCs, but higher than both MA-NCs/PMMA blend (ca. 54%) and previously reported encapsulated NCs (APTES-/NH_2-POSS-$CH_3NH_3PbBr_3$: 15-55%, POSS-$CsPbBr_3$: 61%).[16, 28] The longer lifetime (404 nm, excitation wavelength) observed in the PMPOPNC film (Figure S10) is attributed to decreased surface defect density as a result of better surface ligand passivation.[22, 32] Furthermore, the emission wavelength of the PMPOPNC composite materials can be readily tuned throughout the entire visible spectral region by adjusting the ratio of halides in the colloidal $CsPbX_3$ NCs (X=Cl, Br and I).[7, 8]

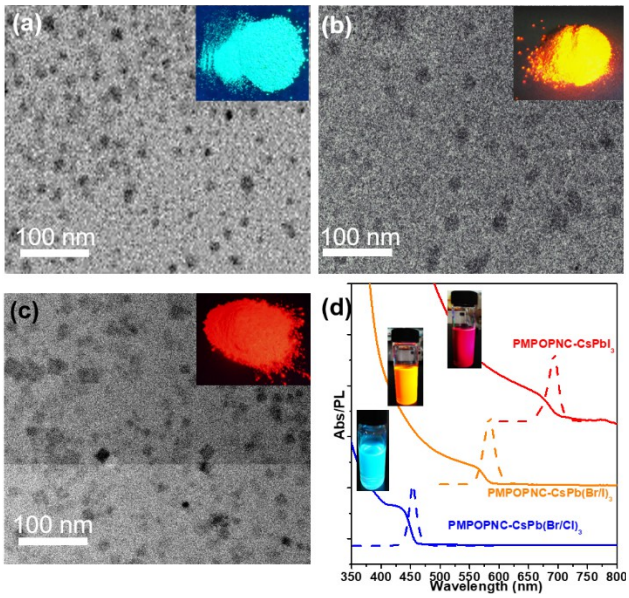


Figure 5. TEM images of (a) PMPOPNC-$CsPb(Br/Cl)_3$, (b) PMPOPNC-$CsPb(Br/I)_3$, and (c) PMPOPNC-$CsPbI_3$. Inset images are the corresponding photographs of the powders under UV light. (d) UV-vis and PL spectra of PMPOPNC-$CsPbX_3$ synthesized with various Cl/Br/I ratios. Photographs of the respective colloidal solutions under UV light are shown in the inset.

Similarly, the PMPOPNC composites with various colors can be readily obtained by using different lead halide precursors (from mixtures of $PbCl_2$/$PbBr_2$ (1:1), $PbBr_2$/PbI_2 (1:1), and pure PbI_2 instead of $PbBr_2$) in the nanocrystal synthesis to afford blue (452 nm emission, PLQY = 67%), yellow (585 nm emission, PLQY = 74%) and red (690 nm emission, PLQY = 69%) fluorescent materials (Figure 5a-c). Corresponding TEM images show the formation of uniform crystalline nanoparticles embedded within the polymer matrix, with the average NCs diameters of 12-18 nm (Figure 5a-c).

The as-synthesized PMPOPNC powder displays a light yellow color under ambient light and bright green fluorescence under UV irradiation (Figure 6a). Notably, the PMPOPNC composite can be well dispersed in various organic solvents to give dispersions with good colloidal stability. This dispersity enables use of the solutions as fluorescent inks, compatible with large area solution fabrication and patterning of thin films. The simple writing process demonstrates a clear route to commercialization and applications in anti-counterfeiting security inks and light emitting displays.

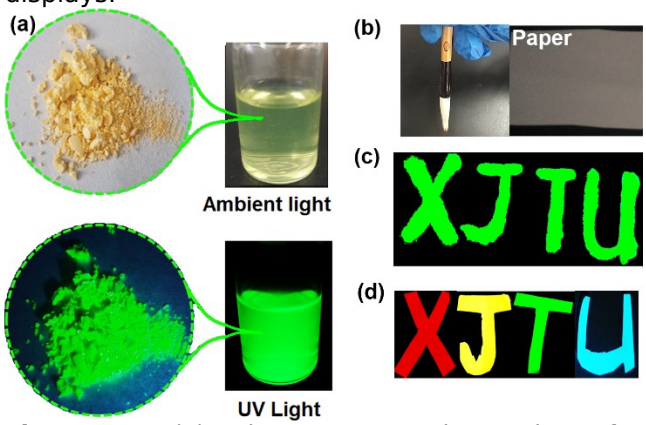


Figure 6. (a) The as-prepared powder of PMPOPNC under ambient light and UV light, showing a yellow color and bright green fluorescence, respectively. (b) Photograph of the brush and a piece of filter paper used for pattern. (c) Photograph of handwritten “XJTU” pattern on a piece of filter paper irradiated by UV light using PMPOPNC solution in toluene as ink after immersion in water for 3h. (d) Photograph of a “XJTU” pattern made from highly luminescent PMPOPNCs containing NCs of MA-$CsPbI_3$, MA-$CsPbI_{1.5}/Br_{1.5}$, MA-$CsPbBr_3$ and MA-$CsPbCl_{1.5}/Br_{1.5}$ under UV light.

As a demonstration, a four-letter “XJTU” pattern was handwritten on a piece of filter paper using a brush (Figure 6b, also with the photograph of the brush), which is nearly colorless under room light but exhibits excellent uniformity and strong PL emission under UV light. The high PL emission can be preserved even under immersion in water for 3 h, thanks to the protective POSS-based polymer layer (Figure 6c). As demonstrated in Figure 6d, a similar pattern that emits bright red, yellow, green and cyan colors is casted from PMPOPNC composites with the following NC halide compositions, respectively: $CsPbI_3$, $CsPbI_{1.5}/Br_{1.5}$, $CsPbBr_3$ and $CsPbCl_{1.5}/Br_{1.5}$.

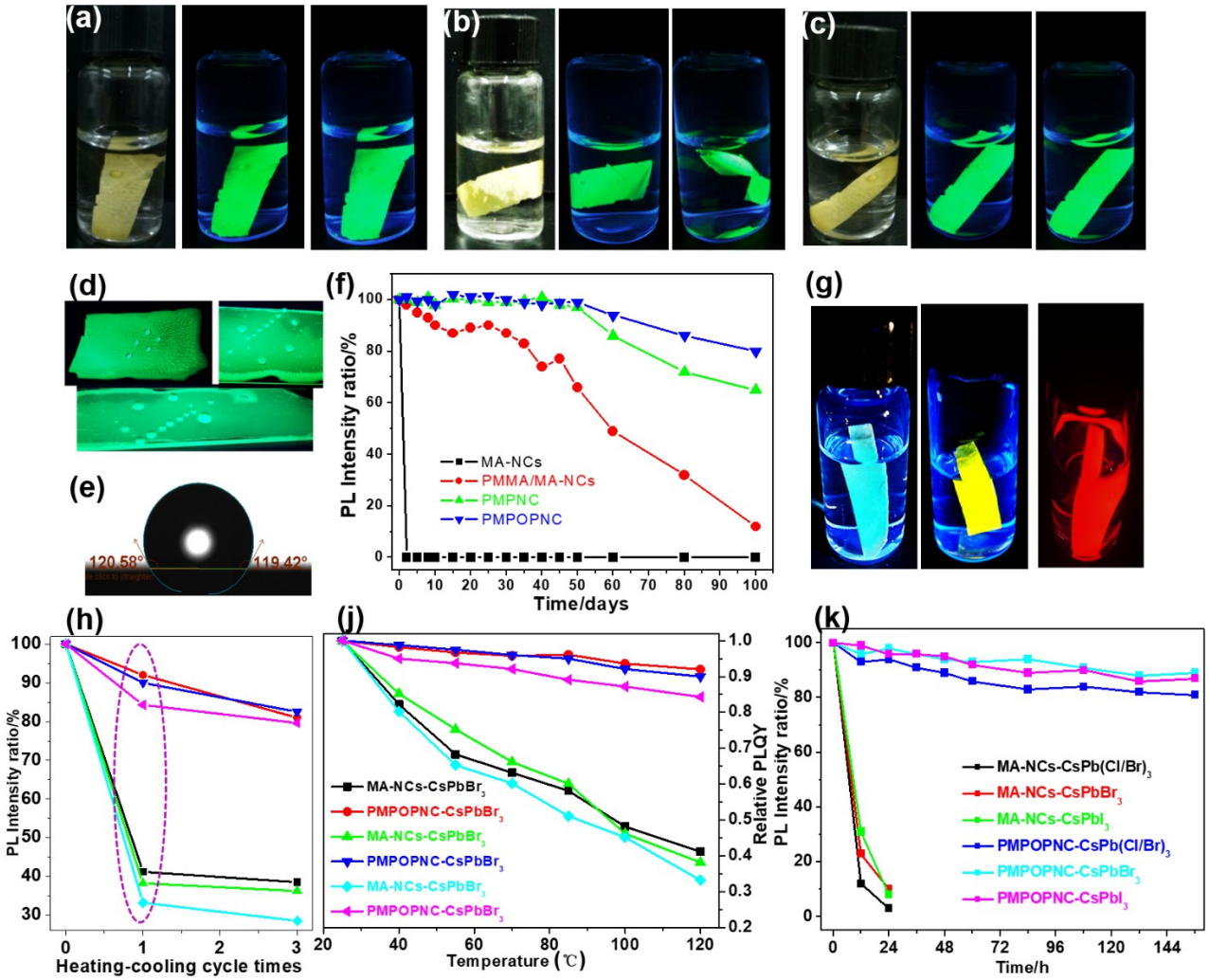


Figure 7. (a-c) Photographs taken under ambient light or UV irradiation at indicated time period after immersion in water of thin films of MA-NC/PMMA blend, PMPNC and PMPOPNC films, respectively. (d and e) Photos showing the hydrophobicity of PMPOPNC film. (f) The relative PLQY plots of MA-NC, MA-NC/PMMA blend, PMPNC and PMPOPNC films upon immersing in water over time. (g) Photographs of films of PMPOPNC-CsPb(Br/Cl)$_3$, PMPOPNC-CsPb(Br/I)$_3$ and PMPOPNC-CsPbI$_3$ taken under UV irradiation after immersion in water for 60 days. (h) The relative PLQY plots of free MA-NCs and PMPOPNC films of various colors upon heating/cooling (room temperature/120 ˚C) for 3 cycles. (j) The relative PLQY plots against temperature after the 1st cycle. (k) The relative PLQY plots against different UV irradiation times.

Perovskite nanocrystals $CsPbX_3$ (X=Cl, Br, I) are easily degraded by ambient humidity and upon contact with polar solvents.[16, 34, 45] The copolymers from hydrophobic monomers of MMA and MA-POSS are expected to provide excellent dewetting properties,[42] thus lending stability to specific copolymerized composites. The luminescence of MA-NCs quenched completely after immersing in water in 1 hour (Figure S11). The water-resistance of the composites films was also tested by immersing the films in deionized water over different periods of time (Figure 7a-c and Table S1). The relative PL of the thin film of MA-NCs/PMMA blend decayed to 87% and 49% of its initial value after 30 and 60 days, respectively. Much higher PL stability was observed for PMPNC and PMPOPNC composites films, which displayed less than 5% decay of PLQY after immersing in water for 60 days (Figure 7f). PXRD spectrum of the sample immersed in water for 70 days displayed -discernible diffraction patterns that were derived from the NCs and the POSS cages despite a decreased signal-to-noise ratio (Figure S12), which were attributable to migration and re-orientation of POSS moieties onto the top surface of the film.

It is well known that in POSS-based copolymers, the POSS fraction is prone to migrate to the air-solid interface, resulting in hydrophobic surfaces and morphologies with micro-nano roughness features.[37, 41, 42] XPS analysis of the PMPOPNC film (Figure S5) reveals that the surface Si content is significantly higher than that from the corresponding PMPOPNC powder, while the surface Pb, Cs and Br concentrations decrease significantly (Figure 3c-h). These results suggest that the low-energy POSS fraction of the polymer is sequestered onto the surface,

which also leads to rough surface morphology as observed by the SEM studies (Figure S8). The resulting surface is rather hydrophobic, as suggested by a static water contact angle of 120° (Figure 7d and e). This contact angle is significantly larger than that of the films of PMPNC (105°) and MA-NCs/PMMA (104°). These results collectively suggest that the POSS fraction migrates to the surface and acts as a block barrier to water permeation.[16, 42]

The stability of PMPOPNC film towards protic and aprotic solvents was also tested by immersion in common solvents such as water, methanol, ethanol and hexane. The PL remains unaffected after two months, attesting to the excellent solvent resistance of the composite films (Figure S13). The thermal stability was also tested by heating to 120 °C and cooling to room temperature (repeated for 3 cycles). Photographs in Figure 7g confirm that the thin films of PMPOPNC-$CsPb(Br/Cl)_3$, PMPOPNC-$CsPb(Br/I)_3$ and PMPOPNC-$CsPbI_3$ remain highly fluorescent after immersion in water for 60 days. As shown in Figure 7h, PMPOPNC has shown greater retention of its luminescence when compared to the MA-NCs after heat cycling. Colloidal solutions of MA-NCs degrade dramatically upon heating. At 120 °C, less than 40% of original PL intensity was maintained. In contrast, the PMPOPNC films retain more than 80% of their PLQY after heating to 120°C (Figure 7j). The PMPOPNC composite also has demonstrated enhanced photostability relative to the neat NCs. Thin films of PMPOPNC composites of $CsPbBr_3$, $CsPbI_3$ or $CsPb(Cl/Br)_3$ were irradiated under blue light. After 24 h, no measurable PL intensity decrease was observed for the PMPOPNC films while the PL of the neat NCs were severely quenched. After 156 h, ~81% of the initial PL intensity was still maintained (Figure 7k). No PL peak shift was detected (Figure S14), indicating that the NCs are encapsulated inside the polymers and well separated from each other to preclude fusion and aggregation.

Additionally, the tendency to anions exchange is completely suppressed for the PMPOPNC films. No change of emission properties was observed after exposing the PMPOPNC films to chloride or iodide solution (Figure S15), in sharp contrast to the free $CsPbBr_3$ NC thin films.[7, 8, 18] All these results collectively demonstrate that the copolymerization approach to embedding $CsPbBr_3$ NCs in POSS-based polymer matrixes is superior in stabilizing the NCs by providing a POSS permeation barrier to shield environmental agents.

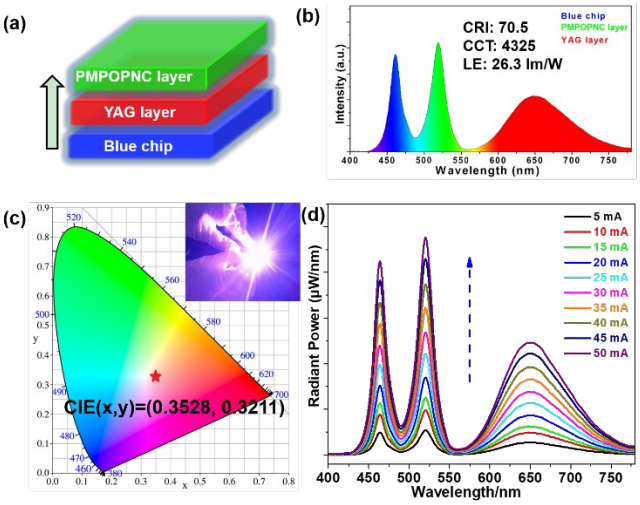


Figure 8. (a) Schematics of the WLED, composed of GaN blue (460 nm) LED chips, PMPOPNC films and YAG powder mixed with silicone resin as the blue, green and red light source. (b) EL emission spectra of the WLED. (c) CIE color coordinates of the fabricated devices with PMPOPNC composite films. Insert in (c) Photograph of a working device with an applied current of 20 mA. (d) EL spectra of fabricated WLED under various operation currents.

In order to demonstrate that the stable PMPOPNC ink is suitable for photonic applications, films were cast from the toluene solution and subsequently employed as the green fluorophore in a white light emitting device(WLED).[50] Figure 8 illustrates the typical WLED device structure, in which the PMPOPNC, YAG powder and GaN backlight were used as the green, red and blue sources. The electroluminescence (EL) spectrum of the prepared WLED device presents broad green and red emission peaks at 516 nm and 660 nm excited by the 460 nm GaN LED, attributed to the respective emission bands of PMPOPNC film and YAG phosphor.

The optimized WLED device exhibits a color rendering index (CRI) of 70.5, a low correlated color temperature (CCT) of 4325 K and a luminous efficacy (LE) of 26.3 lm/W at an operating current of 20 mA. Saturated and bright white emission can be clearly observed when the device is operated, with a CIE color coordinate (0.353, 0.321), very close to standard white emission (0.33, 0.33). The color is stable at currents between 5 and 50 mA, indicating that the perovskite composite is a valuble light emitter even at high current densities (Figure 8d). The solution processability, together with the improved stability verifies the great potential of the PMPOPNC composite as a promising fluorescent ink for solution processable fabrication of wide-color gamut lighting and display devices.

Conclusion

By using methacrylic acid in place of oleic acid, we have synthesized homogenous $CsPbX_3$ NCs with a size of 14-17 nm and 85% PLQY featuring bound cross-linkable monomers as surface ligands. The functionalized NCs undergo UV-initiated copolymerization with various methacrylic ester co-monomers. The

key to the success of the polymerization is to circumvent the common degradation and fusion of $CsPbX_3$ NCs, realized by using CBr_4 as a bromide source to provide a bromide-rich medium to passivate surface defects in situ. This protocol provides a general strategy for the fabrication of NC-polymer composites that feature homogenously encapsulated NCs in the polymer matrix, well preserved fluorescent properties and high solution processability, as demonstrated in the copolymers of MMA and MA-POSS monomers. The composite PMPOPNC exhibited a higher PLQY than free $CsPbBr_3$ NCs and previously reported encapsulated NCs. The POSS fraction also serves as a permeation barrier, and the composite displayed extraordinary chemical stability towards water and other solvents along with enhanced thermal stability. In addition, the PMPOPNC composite can be dispersed in organic solvents to form easily processable inks, facilitating spin coating and, in this example, use in a white down-converting LED. This work provides an effective and general approach to enhancing the perovskite NC's stability by *co*-polymerization with hydrophobic POSS monomers. Stable and durable perovskite-based fluorescent inks open the door to a previously unlikely range of practical use of $CsPbX_3$ perovskite nanocrystals for high-performance optoelectronic devices.

Experimental Section

Materials and Chemicals: $PbBr_2$ (99.90%), Cs_2CO_3 (99.99%), CBr_4 (99.99%), methacrylic acid (MA), octadecene (ODE, 90%), oleic acid (OA, 90%, AR) and oleylamine (OLA, 90%, AR) were purchased from Aladdin and used as received without purification. 2,2-Azobisisobutyronitrile (AIBN) is recrystallized in methanol twice and kept in a vacuum oven before use. Methacrylisobutyl POSS (MA-POSS, Mw=947.3 $g \cdot mol^{-1}$) were purchased from Hybrid Plastics Co. (USA) and used as received. Silicone resin and phosphor fluorescent powder (red) were purchased from Shenzhen looking long technology co., LTD and used as received without purification. Methyl methacrylate (MMA, 99 wt%) (Aldrich) was rinsed by 5 wt% NaOH aqueous solution and ion-free water until the rinsed water reached a pH of 7, which was followed by drying over CaH_2 for 24 h and distilling under reduced pressure to remove the inhibitor before use. All the other solvents were used as received without any purification.

Synthesis of MA-$CsPbBr_3$ Nanocubes (MA-NCs): MA-$CsPbBr_3$ nanocubes were prepared following a modified procedure.[5] ODE (5 mL) and $PbBr_2$ (0.188 mmol, 0.069 g, or certain amount of PbI_2, $PbBr_2/PbI_2$ and $PbCl_2/PbBr_2$) were loaded into a 25 mL 3-neck flask and dried under vacuum for 1 h at 120 °C. Equimolar organic acid and base pairs were pre-mixed with the following stoichiometry: MA-OAm (methacrylic acid, 0.14 g, and oleylamine, 0.50 mL) and MA-HAm (methacrylic acid, 0.14 g, and hexylamine, 0.21 ml). The acid/amine mixture were dried and injected at 120 °C under N_2. It should be noted that both the acid and base have to be present in order for complete dissolution of the $PbBr_2$ solid. After complete dissolution was achieved, the temperature was raised to the desired temperature of 150 °C under N_2, followed by quick injection of the cesium oleate solution (Cs_2CO_3/acid, 0.4 mL, 0.125 M in ODE). Five seconds later, the reaction mixture was cooled to room temperature by an ice/water bath. The crude solution was directly centrifuged at 3000 round per minute (rpm) to remove impurities and large particles. After that, the supernatant was subjected to high-speed centrifugation at 10000 rpm for 10 min by collecting and re-dispersing in either pure hexane or hexane/acetone mixture (hexane:acetone=0.7:0.3 by volume).[10] The centrifugation/re-dispersion procedure was repeated three to five times, after which the solid precipitate was collected and re-dispersed in toluene or hexane for further characterization.

Bleaching test by UV light irradiation: The colloidal solutions of MA-NCs (2 ml, 0.5 mg mL^{-1} in toluene) and MA-NCs with CBr_4 (2 ml, 0.5 mg mL^{-1} in toluene + 20 mg CBr_4) were stored in two different flasks at room temperature and subjected to UV light irradiation (365 nm, 0.5 $W \cdot cm^{-2}$) over different period of times. The aged solutions were then subjected to further characterization.

Synthesis of PMPOPNC by photo-initiation: The photo-polymerization was prepared by using MMA or a mixture of MMA and MA-POSS as monomers and AIBN as initiator at room temperature (RT). A typical synthesis procedure is described in Scheme 1. After a flask filled with AIBN was degassed three times by vacuum/nitrogen gas, a mixture of MMA (3 ml, or 2 ml MMA and 1 g MA-POSS), MA-NC (1 ml, 0.5 mg mL^{-1} in toluene), CBr_4 (5 mg) and toluene (5 ml) was injected gradually. The polymerization was carried out under UV-light irradiation (365 nm, 0.5$W \cdot cm^{-2}$) at RT for 1 h. After that, the colorless solution is poured into n-hexane to precipitate the product. The precipitate was purified by first dissolving in toluene and re-precipitating into hexane for three times. The free NCs, excess AIBN and free monomers of MMA and MA-POSS are soluble in hexane and can be removed from the supernatant after centrifugation. The PMPOPNC composite was dried in a vacuum oven overnight before being stored for future use (yield: 65 %).

Preparation of PMPOPNC composite based ink and its use for writing patterns: Under stirring, PMPOPNC powder (50 mg) was dispersed in toluene (1 g, a weight ratio of

4.8% wt). The resultant solution was handwritten onto filter papers using an ink brush.

PMPOPNC Film: For the composite thin film, the PMPOPNC powder was dissolved in toluene at a concentration of 0.1 g mL^{-1}, and the solution was spin-coated (500 rpm, 30 s) onto a glass substrate. The copolymer composite films were kept in a vacuum oven for further measurements.

PMPOPNC Matrix: The PMPOPNC powder was dissolved in toluene at a concentration of 0.2 $g{\cdot}mL^{-1}$. Then, the solution was poured into a glass dish for drying. The composite matrixes containing NCs of MA-$CsPbI_3$, MA-$CsPbI_{1.5}/Br_{1.5}$, MA-$CsPbBr_3$ and MA-$CsPbCl_{1.5}/Br_{1.5}$ were sheared into “X”, “J”, “T” and “U” alphabetic symbols, respectively.

Stability Tests: For water stability test, all composites of PMPOPNC films were immersed in de-ion water at RT for measurements at different times. For different solvents resistant test, all composites of PMPOPNC films with rectangles were immersed in water, methanol, ethanol, hexane at RT for measurements over times. For thermal stability test, films of PMPOPNC were placed on a heating plate for several heating/cooling cycles (room temperature/120 °C), of which PL intensities were analyzed.

White emitting LED device fabrication: White emitting LED were made by spin casting the green PMPOPNC (516 nm) and the red YAG fluorescent (660 nm) solutions onto a blue (460 nm) emitting GaN LED backlight. First, the powdered YAG phosphors (0.3 g) was dispersed in silicon resin (3 g) with vigorous stirring. The resulting mixture was directly spin coated onto blue LED chips and thermally cured, at 40 °C for 30 min and then 120 °C for 60 min, to yield a red emitting layer. A PMPOPNC film was spun-cast from toluene on top of the cured YAG film, which would be stowage onto the upper surface of YAG-based LED devices by mixing with silicon resin, Final device stacks were thermally cured at 40 °C for 30 min and then 120 °C for 60 min, to yield a white emitting device.

Characterization Methods: ^{1}H-NMR spectra were recorded on a Bruker Avance II 500 MHz NMR Spectrometer operating at ^{1}H frequency of 500 MHz and equipped with BBFO-Z probe. Ultraviolet and visible absorption (UV-vis) spectra of colloidal solutions were collected using a Cary 5000 UV-Vis-NIR spectrophotometer. Fluorescence spectra, photoluminescence fluorescent lifetime and absolute photo-luminescent quantum yields (PLQYs) collected by using an integrated sphere, were recorded on an Edinburgh Instruments FLS920 spectrophotometer. PXRD data were acquired using a Bruker AXS D8 Discover X-Ray Diffractometer at a wavelength of Cu K (1.79 Å). X-Ray photoelectron spectroscopy (XPS) measurement for elemental composition was processed on the air-exposed composites film surface and composites powder by an AXIS ULTRA (England, KRATOS ANALYTICAL Ltd) using an Al mono Kα X-ray source (1486.6 eV) operated at 150 W. Measurements were performed in hybrid mode using electrostatic and magnetic lenses, and the take-off angle was 0°. The spectra were collected at fixed analyzer pass energies of 160 and 20 eV, respectively. Samples were mounted in floating mode in order to avoid differential charging. Charge neutralization was required for all samples. All the spectra were calibrated to the C 1s peak at binding energies of 284.8 eV of the sp^3 hybridized (C-C) carbon. The data were analyzed with commercially available software, Casa XPS. The individual peaks were fitted by a Gaussian(70%)-Lorentzian (30%) (GL30) function after linear or Shirley-type background subtraction. SEM images were acquired on a JEOL 7800F Field Emission Scanning Electron Microscope. TEM and high-resolution TEM (HR-TEM) data were acquired on a FEI G_2F_{30} electron microscope operated at 200 kV with a Gatan SC 200 CCD camera. The surface contact angle measurements were conducted at 25 °C on an OCA-20 DataPhysics Instruments GmbH with SCA 20 software. The results were based on the average of at least five measurements

Supporting Information

^{1}HNMR and IR spectra of MA and $CsPbBr_3$ NCs; TEM, HR-TEM, SEM, XPS, XRD, PL, TGA of PMMA/MA-NCs, PMPNC and PMPOPNC; The stability test of free MA-NC and PMPOPNC films in water, methanol, ethanol and hexane. Table of the water contact angle and the relative PLQY values of MA-NC/PMMA, PMPNC and PMPOPNC. Anion exchange experiments of free $CsPbX_3$ and PMPOPNC films. This material is available free of charge via the Internet at http://pubs.acs.org.

AUTHOR INFORMATION

Corresponding Author

*Email: heling@mail.xjtu.edu.cn.
*Email: yliu@lbl.gov.

Author Contributions

All authors have given approval to the final version of the manuscript.

Notes

The authors declare no competing financial interest.

ACKNOWLEDGMENT

This work was supported by the National Natural Science Foundation of China (NSFC Grants 51373133, 51573145), the China Postdoctoral Science Foundation Funded Project (2017M623149) and the Foundation of Xi'an Jiao Tong University for New Teachers (HX1K020). This work was also supported by the U.S. Department of Energy, Office of Science, Office of Basic Energy

Sciences, Materials Sciences and Engineering Division, under Contract No. DE-AC02-05-CH11231 within the Inorganic/Organic Nanocomposites Program (KC3104) (MJ and YL). Work at the Molecular Foundry was supported by the Office of Science, Office of Basic Energy Sciences, of the U.S. Department of Energy under Contract No. DE-AC02-05CH11231. The authors also wish to express their gratitude to the MOE Key Laboratory for Nonequilibrium Condensed Matter and Quantum Engineering of Xi'an Jiaotong University. The authors kindly thank Guijiang Zhou, Xiaolong Yang, Boao Liu and Juan Yang in Xi'an Jiaotong University for useful discussions.

REFERENCES

(1) Grancini, G.; Srimath Kandada, A. R.; Frost, J. M.; Barker, A. J.; De Bastiani, M.; Gandini, M.; Marras, S.; Lanzani, G.; Walsh, A.; Petrozza, A. Role of Microstructure in the Electron-Hole Interaction of Hybrid Lead-Halide Perovskites. *Nat. Photonics* **2015**, *9*, 695-701.
(2) Yakunin, S.; Protesescu, L.; Krieg, F.; Bodnarchuk, M. I.; Nedelcu, G.; Humer, M.; De Luca, G.; Fiebig, M.; Heiss, W.; Kovalenko, M. V. Low-threshold amplified spontaneous emission and lasing from colloidal nanocrystals of caesium lead halide perovskites. *Nat. Commun.* **2015**, *6*, 8056-8063.
(3) Yuan, Z.; Zhou, C.; Tian, Y.; Shu, Y.; Messier, J.; Wang, J. C.; van de Burgt, L. J.; Kountouriotis, K.; Xin,Y.; Holt, E.; Schanze, K.; Clark, R.; Siegrist, T.; Ma, B. One-dimensional organic lead halide perovskites with efficient bluish white-light emission. *Nat. Commun.* **2017**, *8*, 14051-14057.
(4) Veldhuis, S. A.; Boix, P. P.; Yantara, N.; Li, M.; Sum, T. C.; Mathews, N.; Mhaisalkar, S. G. Perovskite Materials for Light-Emitting Diodes and Lasers. *Adv. Mater.* **2016**, *28,* 6804-6834.
(5) Protesescu, L.; Yakunin, S.; Bodnarchuk, M. I.; Krieg, F.; Caputo, R.; Hendon, C. H.; Yang, R. X.; Walsh, A.; Kovalenko, M. V. Nanocrystals of Cesium Lead Halide Perovskites ($CsPbX_{(3)}$, X =Cl, Br, and I): Novel Optoelectronic Materials Showing Bright Emission with Wide Color Gamut. *Nano Lett.* **2015**, *15,* 3692-3696.
(6) Swarnkar, A.; Chulliyil, R.; Ravi, V. K.; Irfanullah, M.; Chowdhury, A. Colloidal $CsPbBr_3$ Perovskite Nanocrystals: Luminescence beyond Traditional Quantum Dots. Nag, A. *Angew. Chem. Int. Ed.* **2015**, *54*, 15424-15428.
(7) Akkerman, Q. A.; D'Innocenzo, V.; Accornero, S.; Scarpellini, A.; Petrozza, A.; Prato, M.; Manna, L. Tuning the Optical Properties of Cesium Lead Halide Perovskite Nanocrystals by Anion Exchange Reactions. *J. Am. Chem. Soc.* **2015**, *137,* 10276-10281.
(8) Nedelcu, G.; Protesescu, L.; Yakunin, S.; Bodnarchuk, M. I.; Grotevent, M. J.; Kovalenko, M. V. Fast Anion-Exchange in Highly Luminescent Nanocrystals of Cesium Lead Halide Perovskites ($CsPbX_3$, X = Cl, Br, I). *Nano Lett.* **2015**, *15,* 5635-5640.
(9) Wang, Y.; Li, X.; Song, J.; Xiao, L.; Zeng, H.; Sun, H. All-Inorganic Colloidal Perovskite Quantum Dots: A New Class of Lasing Materials with Favorable Characteristics. *Adv. Mater.* **2015**, *27,* 7101-7108.
(10) Pan, A.; He, B.; Fan, X.; Liu, Z.; Urban, J. J.; A. Alivisatos, P. L.; Liu, He, Y. Insight into the Ligand-Mediated Synthesis of Colloidal $CsPbBr_3$ Perovskite Nanocrystals: The Role of Organic Acid, Base, and Cesium Precursors. *ACS Nano* **2016**, *10,* 7943-7954.
(11) Sun, S.; Yuan, D.; Xu, Y.; Wang, A.; Deng, Z. Ligand-Mediated Synthesis of Shape-Controlled Cesium Lead Halide Perovskite Nanocrystals via Reprecipitation Process at Room Temperature. *ACS Nano* **2016**, *10,* 3648-3657.
(12) Seth, S.; Samanta, A. A Facile Methodology for Engineering the Morphology of $CsPbX_3$ Perovskite Nanocrystals under Ambient Condition. *Sci Rep,* **2016**, *6*, 37693-37699.
(13) Leijtens, T.; Eperon, G. E.; Noel, N. K.; Habisreutinger, S. N.; Petrozza, A.; Snaith, H. J. Stability of Metal Halide Perovskite Solar Cells. *Adv. Energy Mater.* **2015**, *5*, 1500963-1500985.
(14) Huang, S.; Li, Z.; Wang, B.; Zhu, N.; Zhang, C.; Kong, L.; Zhang, Q.; Shan, A.; Li, L. Morphology Evolution and Degradation of $CsPbBr_3$ Nanocrystals under Blue Light-Emitting Diode Illumination. *ACS Appl. Mater. Inter.* **2017**, *9,* 7249-7258.
(15) Zhang, H.; Wang, X.; Liao, Q.; Xu, Z.; Li, H.; Zheng, L.; Fu, H. Embedding Perovskite Nanocrystals into a Polymer Matrix for Tunable Luminescence Probes in Cell Imaging. *Adv. Funct. Mater.* **2017**, *27,* 1604382-1604389.
(16) Huang, H.; Chen, B.; Wang, Z.; Hung, T. F.; Susha, A. S.; Zhong, H.; Rogach, A. L. Water resistant $CsPbX_3$ nanocrystals coated with polyhedral oligomeric silsesquioxane and their use as solid state luminophores in all-perovskite white light-emitting devices. *Chem. Sci.* **2016**, *7,* 5699-5703.
(17) Dang, Z.; Shamsi, J.; Palazon, F.; Imran, M.; Akkerman, Q. A.; Park, S.; Bertoni, G.; Prato, M.; Brescia, R.; Manna, L. In Situ Transmission Electron Microscopy Study of Electron Beam-Induced Transformations in Colloidal Cesium Lead Halide Perovskite Nanocrystals. *ACS Nano* **2017**, *11,* 2124-2132.
(18) Parobek, D.; Dong, Y.; Qiao, T.; Rossi, D.; Son, D. H. Photoinduced Anion Exchange in Cesium Lead Halide Perovskite Nanocrystals. *J. Am. Chem. Soc.* **2017**, *139*, 4358-4361.
(19) Kim, Y.; Yassitepe, E.; Voznyy, O.; Comin, R.; Walters, G.; Gong, X.; Kanjanaboos, P.; Nogueira, A. F.; Sargent, E. H. Efficient Luminescence from Perovskite Quantum Dot Solids. *ACS Appl. Mater. Inter.* **2015**, *7*, 25007-25013.
(20) Sun, J. Y.; Rabouw, F. T.; Yang, X.-F.; Huang, X.-Y.; Jing, X. P.; Ye, S.; Zhang, Q.-Y. Facile Two-Step Synthesis of All-Inorganic Perovskite $CsPbX_3$ (X= Cl, Br, and I) Zeolite-Y Composite Phosphors for Potential Backlight Display Application. *Adv. Funct. Mater.* **2017**, *27*, 1704371-1704378.
(21) Loiudice, A.; Saris, S.; Oveisi, E.; Alexander, D. T. L.; Buonsanti, R. $CsPbBr_3$ QD/AlOx Inorganic Nanocomposites with Exceptional Stability in Water, Light, and Heat. *Angew. Chem. Int. Ed. Engl.* **2017**, *56,* 10696-10701.
(22) Wei, Y.; Deng, X.; Xie, Z.; Cai, X.; Liang, S.; Ma, P. a.; Hou, Z.; Cheng, Z.; Lin, J. Enhancing the Stability of Perovskite Quantum Dots by Encapsulation in Crosslinked Polystyrene Beads via a Swelling-Shrinking Strategy toward Superior Water Resistance. *Adv. Funct. Mater.* **2017**, *27*, 1703535-1703542.
(23) Xuan, T.; Yang, X.; Lou, S.; Huang, J.; Liu, Y.; Yu, J.; Li, H.; Wong, K. L.; Wang, C.; Wang, J. Highly stable $CsPbBr_3$ quantum dots coated with alkyl phosphate for white light-emitting diodes. *Nanoscale* **2017**, *9*, 15286-15290.
(24) Pan, J.; L. Quan, N.; Zhao, Y.; Peng, W.; Murali, B.; Sarmah, S. P.; Yuan, M.; Sinatra, L.; Alyami, N. M.; Liu, J.; Yassitepe, E.; Yang, Z.; Voznyy, O.; Comin, R.; Hedhili, M. N.; Mohammed, O. F.; Lu, Z. H.; Kim, D. H.;

Sargent, E. H.; Bakr, O. M. Highly Efficient Perovskite-Quantum-Dot Light-Emitting Diodes by Surface Engineering. *Adv. Mater.* **2016**, *28,* 8718-8725.
(25) Gomez, L.; Weerd, C. de; Hueso, J. L.; Gregorkiewicz, T. Color-stable water-dispersed cesium lead halide perovskite nanocrystals. *Nanoscale* **2017**, *9*, 631-636.
(26) Yang, S.; Wang, Y.; Liu, P.; Cheng, Y.-B.; Zhao, H. J.; Yang, H. G. Functionalization of perovskite thin films with moisture-tolerant molecules. *Nat. Energy* **2016**, *1*, 15016-15022.
(27) Palazon, F.; Akkerman, Q. A.; Prato, M.; Manna, L. X-ray Lithography on Perovskite Nanocrystals Films: From Patterning with Anion-Exchange Reactions to Enhanced Stability in Air and Water. *ACS Nano* **2016**, *10*, 1224-1230.
(28) Luo, B.; Pu, Y. C.; Lindley, S. A.; Yang, Y.; Lu, L.; Li, Y.; Li, X.; Zhang, J. Z. Organolead Halide Perovskite Nanocrystals: Branched Capping Ligands Control Crystal Size and Stability. *Angew. Chem. Int. Ed. Engl.* **2016**, *55*, 8864-8868.
(29) Lou, S.; Xuan, T.; Yu, C.; Cao, M.; Xia, C.; Wang, J.; Li, H. Nanocomposites of $CsPbBr_3$ perovskite nanocrystals in an ammonium bromide framework with enhanced stability. *J. Mater. Chem. C* **2017**, *5*, 7431-7435.
(30) Di, X.; Hu, Z.; Jiang, J.; He, M.; Zhou, L.; Xiang, W.; Liang, X. Use of long-term stable $CsPbBr_3$ perovskite quantum dots in phospho-silicate glass for highly efficient white LEDs. *Chem. Commun.* **2017**, *53*, 11068-11071.
(31) Raja, S. N.; Bekenstein, Y.; Koc, M. A.; Fischer, S.; Zhang, D.; Lin, L.; Ritchie, R. O.; Yang, P.; Alivisatos, A. P. Encapsulation of Perovskite Nanocrystals into Macroscale Polymer Matrices: Enhanced Stability and Polarization. *ACS Appl. Mater. Inter.* **2016**, *8*, 35523-35533.
(32) Sun, H.; Yang, Z.; Wei, M.; Sun, W.; Li, X.; Ye, S.; Zhao, Y.; Tan, H.; Kynaston, E. L.; Schon, T. B.; Yan, H.; Lu, Z. H.; Ozin, G. A.; Sargent, E. H.; Seferos, D. S. Chemically Addressable Perovskite Nanocrystals for Light-Emitting Applications. *Adv. Mater.* **2017**, *29*, 1701153-1701161.
(33) Wang, Y.; He, J.; Chen, H.; Chen, J.; Zhu, R.; Ma, P.; Towers, A.; Lin, Y.; Gesquiere, A. J.; Wu, S. T.; Dong, Y. Ultrastable, Highly Luminescent Organic-Inorganic Perovskite-Polymer Composite Films. *Adv. Mater.* **2016**, *28*, 10710-10717.
(34) Hai, J.; Li, H.; Zhao, Y.; Chen, F.; Peng, Y.; Wang, B. Designing of blue, green, and red $CsPbX_3$ perovskite-codoped flexible films with water resistant property and elimination of anion-exchange for tunable white light emission. *Chem. Commun*. **2017**, *53*, 5400-5403.
(35) Hou, S.; Guo, Y.; Tang, Y.; Quan, Q. Synthesis and Stabilization of Colloidal Perovskite Nanocrystals by Multidentate Polymer Micelles. *ACS Appl. Mater. Inter.* **2017**, *9*, 18417-18422.
(36) Kuo, S. W.; Chang, F.-C. POSS related polymer nanocomposites. *Prog. Polym. Sci.* **2011**, *36*, 1649-1696.
(37) Ramirez, S. M.; Diaz, Y. J.; Sahagun, C. M.; Duff, M. W.; Lawal, O. B.; Iacono, S. T.; Mabry, J. M. Reversible addition–fragmentation chain transfer (RAFT) copolymerization of fluoroalkyl polyhedral oligomeric silsesquioxane (F-POSS) macromers. *Polym. Chem.* **2013**, *4*, 2230-2234.
(38) Xu, N.; Stark, E. J.; Dvornic, P. R.; Meier, D. J.; Hu, J.; Hartmann-Thompson, C. Hyperbranched Polycarbosiloxanes and Polysiloxanes with Octafunctional Polyhedral Oligomeric Silsesquioxane (POSS) Branch Points. *Macromolecules* **2012**, *45*, 4730-4739.
(39) Cordes, D. B.; Lickiss, P. D.; Rataboul, F. Recent Developments in the Chemistry of Cubic Polyhedral Oligosilsesquioxanes. *Chem. Rev*. **2010**, *110*, 2081-2173.
(40) Wang, F.; Lu, X.; He, C. Some recent developments of polyhedral oligomeric silsesquioxane (POSS)-based polymeric materials. *J. Mater. Chem*. **2011**, *21*, 2775-2782.
(41) Mya, K. Y.; Lin, E. M. J.; Gudipati, C. S.; Shen, L.; He, C. Time-Dependent Polymerization Kinetic Study and the Properties of Hybrid Polymers with Functional Silsesquioxanes. *J. Phys. Chem. B* **2010**, *114*, 9119-9127.
(42) Pan, A.; Yang, S.; He, L.; Zhao, X. Star-shaped POSS diblock copolymers and their self-assembled films. *RSC Adv.* **2014**, *4*, 27857-27866.
(43) De Roo, J.; Ibanez, M.; Geiregat, P.; Nedelcu, G.; Walravens, W.; Maes, J.; Martins, J. C.; Van Driessche, I.; Kovalenko, M. V.; Hens, Z. Highly Dynamic Ligand Binding and Light Absorption Coefficient of Cesium Lead Bromide Perovskite Nanocrystals. *ACS Nano* **2016**, *10*, 2071-81.
(44) Wolcott, A.; Doyeux, V.; Nelson, C. A.; Gearba, R.; Lei, K. W.; Yager, K. G.; Dolocan, A. D.; Williams, K.; Nguyen, D.; Zhu, X. Y. Anomalously Large Polarization Effect Responsible for Excitonic Red Shifts in PbSe Quantum Dot Solids. *J. Phys. Chem. Lett.* **2011**, *2*, 795-800.
(45) Pan, A.; Jurow, M. J.; Qiu, F.; Yang, J.; Ren, B.; Urban, J. J.; He, L.; Liu, Y. Nanorod Suprastructures from a Ternary Graphene Oxide-Polymer-$CsPbX_3$ Perovskite Nanocrystal Composite That Display High Environmental Stability. *Nano Lett.* **2017**, *17*, 6759-6765.
(46) Li, X.; Wang, Y.; Sun, H.; Zeng, H. Amino-Mediated Anchoring Perovskite Quantum Dots for Stable and Low-Threshold Random Lasing. *Adv. Mater.* **2017**, *29*, 1701185-1701193.
(47) Chen, J.; Liu, D.; Al-Marri, M. J.; Nuuttila, L.; Lehtivuori, H.; Zheng, K. Photo-stability of $CsPbBr_3$ perovskite quantum dots for optoelectronic application. *Sci. China Mater.* **2016**, *59*, 719-727.
(48) Wang, Y.; Li, X.; Sreejith, S.; Cao, F.; Wang, Z.; Stuparu, M. C.; Zeng, H.; Sun, H. Photon Driven Transformation of Cesium Lead Halide Perovskites from Few-Monolayer Nanoplatelets to Bulk Phase. *Adv. Mater.* **2016**, *28*, 10637-10643.
(49) Pan, A.; Jurow, M.; Zhao, Y.; Qiu, F.; Liu, Y.; Yang, J.; Urban, J. J.; He, L.; Liu, Y. Templated self-assembly of one-dimensional $CsPbX_3$ perovskite nanocrystal superlattices. *Nanoscale* **2017**, *9*, 17688-17693.
(50) Zhou, Q. C.; Bai Z.; Lu W. G.; Wang Y. T.; Zou B. S.; Zhong H. Z. In Situ Fabrication of Halide Perovskite Nanocrystal-Embedded Polymer Composite Films with Enhanced Photoluminescence for Display Backlights. *Adv. Mater*. **2016**, *28*, 9163-9168.

TOC Graphics

